Geophysical Research Letters

RESEARCH LETTER
10.1029/2022GL097726

Key Points:

- We present the first global assessment of projected changes in compound river flood-hot extremes
- Future flood-hot extremes are mainly driven by changes in hot extremes
- Substantial increases in compound flood-hot extremes are projected in tropical regions

Supporting Information:

Supporting Information may be found in the online version of this article.

Correspondence to:

J. Chen and J. Yin,
jiechen@whu.edu.cn;
jboyn@whu.edu.cn

Citation:

Gu, L., Chen, J., Yin, J., Slater, L. J., Wang, H.-M., Guo, Q., et al. (2022). Global increases in compound flood-hot extreme hazards under climate warming. *Geophysical Research Letters*, *49*, e2022GL097726. https://doi.org/10.1029/2022GL097726

Received 7 JAN 2022
Accepted 5 APR 2022

Author Contributions:

Conceptualization: Lei Gu
Methodology: Lei Gu
Supervision: Jie Chen, Jiabo Yin
Validation: Hui-Min Wang, Qiang Guo, Maoyuan Feng, Hui Qin, Tongtiegang Zhao
Writing – original draft: Lei Gu
Writing – review & editing: Louise J. Slater

Global Increases in Compound Flood-Hot Extreme Hazards Under Climate Warming

Lei Gu[1], Jie Chen[2], Jiabo Yin[2], Louise J. Slater[3], Hui-Min Wang[4], Qiang Guo[5], Maoyuan Feng[6], Hui Qin[1], and Tongtiegang Zhao[7]

[1]School of Civil and Hydraulic Engineering, Huazhong University of Science and Technology, Wuhan, China, [2]State Key Laboratory of Water Resources and Hydropower Engineering Science, Wuhan University, Wuhan, China, [3]School of Geography and the Environment, University of Oxford, Oxford, UK, [4]Department of Civil and Environmental Engineering, National University of Singapore, Singapore, Singapore, [5]Department of Civil Engineering, The University of Tokyo, Tokyo, Japan, [6]College of Urban and Environmental Sciences, Peking University, Beijing, China, [7]Center for Water Resources and Environment, Sun Yat-sen University, Guangzhou, China

Abstract Under global warming, a novel category of extreme events has become increasingly apparent, where flood and hot extremes occur in rapid succession, causing significant damages to infrastructure and ecosystems. However, these bivariate compound flood-hot extreme (CFH) hazards have not been comprehensively examined at the global scale, and their evolution under climate warming remains unstudied. Here, we present the first global picture of projected changes in CFH hazards by using a cascade modeling chain of CMIP6 models, satellite and reanalysis data sets, bias correction, and hydrological models. We find an increasing percentage of floods will be accompanied by hot extremes under climate change; the joint return periods of CFHs are projected to decrease globally, particularly in the tropics. These decreasing joint return periods are largely driven by changes in hot extremes and indicate a likely increase of CFH hazards, and ultimately highlight the urgent need to conduct adaptation planning for future risks.

Plain Language Summary Climate change alters the Earth's energy budget and accelerates the hydrological cycle, bringing new hazards such as temporally compounding flood and hot extremes. Rapid transitions from devastating floods to deadly heat, or vice versa, which used to be rare, are already occurring under the present climate and bring new threats to infrastructure and the public. However, these bivariate CFH hazards have been poorly understood at the global scale, and their future evolution in the context of climate change has not yet been assessed. Here, we provide the first systematic assessment of projected changes and attributions in the multivariate hazards of global flood-hot extremes. We find that the fraction of flooding accompanied by hot extremes could rise markedly under global warming. Changes in hot extremes dominate the exacerbation of global CFH hazards, especially in tropical climate zones. Our study identifies the tropics as the new global hotspot of flood-hot extreme events in a warming future, and reveals an increasing global risk of unexpected sequential wet-hot extremes, highlighting the need to better prepare adaptation and mitigation solutions.

1. Introduction

Weather and water extremes such as extreme heat and flooding occur frequently throughout the world, with annual economic damages of approximately $2.8 and $15.1 billion and total deaths in the thousands since the 1960s (the Georeferenced Emergency Events Database, EM-DAT, http://www.emdat.be). Alongside the occurrence of these univariate extreme events, multiple co-occurring hazards called compound extreme events have also led to unprecedented ecological and socioeconomical damages in recent decades (Chen et al., 2020; Mukherjee & Mishra, 2021; Ridder et al., 2020; Zhou et al., 2019; Zscheischler & Seneviratne, 2017). Compared with univariate extremes, compound extremes usually amplify damages spatially and temporally (Berg et al., 2015; Cai et al., 2020; Schumacher et al., 2019). For example, heavy rainfall and extreme heat might not always be dangerous in isolation, but a rapid succession of the two may in some cases generate devastating impacts (Brida et al., 2013; Ridder et al., 2020). Climate warming complicates the Earth's energy budget and hydrological cycle, bringing more severe compound extremes that arise from complex interactions between physical processes across multiple spatial and temporal scales (Zscheischler & Fischer, 2020; Zascheischler & Lehner, 2021; Zscheischler

et al., 2020). To facilitate adaptation and mitigation strategies, it is important to disentangle future compound hazards, vulnerability, and further risks (Bevacqua et al., 2019; Chen et al., 2021).

Extreme pluvial events and river floods are well-studied at the global scale (Courty et al., 2019; Do et al., 2020; Kemter et al., 2020; Slater et al., 2021; Yin, Guo, Gentine, et al., 2021), but under climate change, a novel temporal cascade of flood-related hazards has become increasingly apparent, where a flood closely follows a hot extreme, or vice versa. Such compound extremes are far more destructive than flooding alone (Cappucci, 2019; You & Wang, 2021; Zhang & Villarini, 2020). Scorching heat distresses both animals and plants, but may also set the stage for subsequent widespread thunderstorms and flash floods, leading to, e.g., livestock losses (Cowan et al., 2019). A recent example was the 2019 Queensland, Australia event, where compound heat and flooding caused over $1.2 billion U.S. in economic losses (Zhang & Villarini, 2020). Similarly, the sudden switch from a flood to a heat extreme can exacerbate damages (Chen et al., 2021; Liao et al., 2021; Matthews et al., 2019). A large flood can overwhelm infrastructure and cause electricity outrages, while a subsequent heatwave can drive air conditioning needs, such that their occurrence in rapid succession may cause destructive socio-economic impacts. A prominent example is the CFH event that hit Japan in July 2018, which led to over 300 deaths and tremendous economic losses (Wang et al., 2019).

There is growing evidence that extreme flooding may be closely associated with extremely hot climate conditions (Lin, 2019). With climate warming, the meandering of Rossby wave packets along the subtropical jet and the intensification of anticyclones can increase the likelihood of CFHs in monsoon regions (Chen & Zhai, 2017; Enomoto et al., 2009). In addition, the increasingly uneven distribution of precipitation in a warming climate also drives greater clustering of CFH events (Pendergrass & Knutti, 2018). Based on observational data sets, Chen et al. (2021) found that compound flood-hot extremes, which were rare in the past, have gradually become increasingly prevalent after 2000 across China because of anthropogenic climate change. Zhang and Villarini (2020) also found that large magnitude floods were prone to be connected with heat stress under warming, potentially leading to increased infrastructure damages and fatalities.

There are two types of sequences in CFHs. In the first case, a flood is likely to be preceded by a hot extreme. Extreme heat forcing can enhance atmospheric instability and promote convective development, resulting in subsequent extreme precipitation and pluvial flooding (Fowler et al., 2021; You & Wang, 2021). Lagged connections between hot extremes and storms may also be driven by large-scale thermodynamics, circulation shifts and land-sea atmospheric feedbacks (Deng et al., 2020; Raghavendra et al., 2019). Conversely, a flood may be followed by a hot extreme. Major tropical cyclones (TCs) can trigger devastating flooding and leave sustained heat that compensate for the fall in air temperature, contributing to the development of a sequential extreme hot event (Liao et al., 2021; Matthews et al., 2019; Parker et al., 2013).

Although analyses of CFHs have gradually become more common, bivariate hazards of CFHs are still poorly understood at a global scale, and their evolution under a warming future remains unknown. Here, by employing a cascade modeling chain which involves 21 CMIP6 (the latest sixth Coupled Model Inter-comparison Project) climate models under three emission scenarios, satellite and reanalysis data sets, a daily bias correction (DBC), and five lumped conceptual hydrological models, we present the first global analysis systematically quantifying changes in the characteristics and bivariate hazards of CFHs, and disentangling how each univariate factors and their dependences influence the likelihood of CFHs in the context of climate change.

2. Materials and Methods

2.1. Materials

We employ a multimodel ensemble containing 21 global climate models (GCMs) from CMIP6 (Table S1 in Supporting Information S1). Variables include daily precipitation and daily maximum, minimum, and average temperature data of one ensemble member ($r1i1p1f1$) per model covering the 30-year historical (1985–2014) and future (2071–2100, under three emission scenarios SSP1-26, SSP2-45, SSP5-85) periods. Following previous work (Bardon et al., 2021; Rhoades et al., 2020; Shi et al., 2021), we select the 2071–2100 period to represent the end-century scenario which fully consider climate change impacts in the far future.

We take historical precipitation data from the Multi-Source Weighted-Ensemble Precipitation, version 2 (MSWEP V2), the first fully global precipitation data set derived by optimally merging a range of gauge, satellite,

and reanalysis estimates, exhibiting realistic spatial patterns in mean, magnitude, and frequency of precipitation (Beck et al., 2019). Since the number of surface weather stations providing long temperature records shows a large decrease starting in 1980 (Menne et al., 2018), we choose the ERA5 (European Center for Medium Range Weather Forecasts Reanalysis 5, Hersbach et al., 2020; Yin, Guo, Gu, et al., 2021) reanalysis temperature data as the observational climatology. Then we estimate catchment-average climate data by using the Thiessen polygon method (Thiessen & Alter, 1911), to calibrate and validate five lumped hydrological models (more details in processing the climate data including the superiority of MSWEP V2 comparing to ERA5 precipitation in hydrological modeling are clarified in Text S1.1 in Supporting Information S1).

We obtain 22,416 river gauge records from a combination of global and national streamflow archives extending from 1900 to 2017 across the globe (Text S1.2 in Supporting Information S1) and select catchments with the following steps. First, we choose catchments with at least 20 years of continuous daily records to satisfy statistical requirements for robustness. Second, we exclude catchments with poor performance in hydrological simulation (i.e., with the Kling-Gupta efficiency metric (KGE; Gupta et al., 2009), in the five candidate hydrological models all smaller than 0.5, in line with previous studies; Almagro et al., 2021; Jiang et al., 2020) and retain 11,690 catchments (Figure S1a in Supporting Information S1). Finally, we omit nested catchments and keep the discharge location with the highest KGE values during both calibration and validation periods in every grid for ease of presentation (2,323 catchments in total, Figure S1b in Supporting Information S1).

2.2. Bias Correction and Hydrological Simulations and Projections

We adjust the bilinearly interpolated climate model outputs by using a hybrid DBC method, which assumes that future biases of GCMs are consistent with the historical biases (Chen et al., 2013; more details see Text S1.3 and Figures S2–S5 in Supporting Information S1). Considering global catchments exhibit diverse climates and underlying surface conditions, a single hydrological model might be unable to capture the runoff generation and concentration regimes adequately. Thus, we choose five hydrological models as candidates: the HMETS model (Martel et al., 2017), HBV model (Bergström & Forsman, 1973), Xinanjiang (XAJ) model (Zhao, 1992), GR4J-6 model (Perrin et al., 2003), and SIMHYD model (Chiew et al., 2002). For each catchment, we employ a cross validation approach that uses odd years for model calibration and even years for model validation (based on a 20-year time window) to calibrate hydrological models following previous studies (Arsenault et al., 2017; Gu et al., 2020). We utilize the shuffled complex evolution optimization algorithm (SCE-UA) which considers both deterministic and random search techniques (Duan et al., 1992) to optimize the free parameters of the hydrological models, using the KGE metric as the objective function. We calibrate the five hydrological models for each catchment and only keep the best-performing model with the highest KGE values (as most representative of local runoff generation and concentration regimes, Figure S6 in Supporting Information S1). Finally, we force the best model by using bias-corrected precipitation and temperature climate simulations and projections (Gu et al., 2020; Yin, Guo, Gentine, et al., 2021), to simulate historical (1985–2014) and future (2071–2100) streamflow (more validation details of bias correction and hydrological modeling are demonstrated in Text 1.4 and Figures S7–S9 in Supporting Information S1).

2.3. Compound Event Analysis

Since hot extremes mainly occur from May to September in the Northern Hemisphere (November to March in the Southern Hemisphere), we only focus on compound events within those months, referred to as the "warm season." Specifically, we use a peak-over-threshold (POT) approach to define the flood and hot extreme event. For each catchment, we define a period of consecutive days during which the daily streamflow (or daily average temperature) exceeds the 90th percentile based on the warm season of the historical period (1985–2014) as a flood event (or a hot extreme). We use the 90th percentile to capture an adequate number of compound events for frequency analysis. With regard to the minimum lengths of each event, we only keep hot extremes longer than three consecutive days since cumulative heat disproportionately affects humans and ecosystems (You & Wang, 2021) while we retain floods equal to or longer than 1 day since short-duration (subdaily and daily) flooding can overwhelm infrastructure (Yin, Guo, Gentine, et al., 2021). Finally, we define a CFH occurs if a flood event is followed or preconditioned by a hot extreme within a 7-day period (the 7-day period refers to before the onset of the flood in the hot extreme-flood sequence and after the cessation of the flood in the flood-hot extreme sequence). It should be noted that the 7-day threshold only refers to the interval time between floods

and hot extremes but does not limit the duration of a flood or a hot extreme. Similar to previous studies (Chen et al., 2021; Liao et al., 2021), we match each flood with the first hot extreme event. We only retain the largest flood accompanied by the same hot extreme to avoid redundancy. We also consider alternative pairing processes such as using the most extreme hot event in the 7-day period instead of the first hot extreme event to match with floods. This yields similar results to the condition that uses the first hot extreme (Figures S10 and S11 in Supporting Information S1).

We estimate cumulative daily streamflow (Q_c) and daily average temperature (t_c) above the thresholds to characterize extreme events to consider both the duration and the intensity of a CFH event:

$$CFH = \left(\sum_{i=a}^{n} Q_i - Q^{90\text{th}}, \sum_{j=b}^{m} t_j - t^{90\text{th}} \right), \quad |a-b| < TI \quad or |n-m| < TI \tag{1}$$

where Q_i (t_j) denotes the daily streamflow of a flood event starting from date a (b) and ending at date n (m); TI denotes the 7-day temporal interval; $Q^{90\text{th}}$ and $t^{90\text{th}}$ represent the flood and hot extremes threshold, respectively.

To assess CFH hazards, we analyze bivariate return periods by using copulas. We initially estimate marginal distributions of floods (F_{Q_c}) and hot extremes (F_{t_c}) by four parametric distributions (P-III, Gamma, Normal, and Weibull; Table S3 in Supporting Information S1). Then we use three candidate copulas (Frank, Gaussian, and Gumbel; Table S3 in Supporting Information S1) to link the best-fitting marginal distributions of floods and hot extremes ($C\left(F_{Q_c}, F_{t_c}\right)$). We choose the Akaike information criterion (AIC; Akaike, 1974) to determine both the best-fitting marginal distributions and associated copulas, and employ the "AND" joint return period (RP) to measure the bivariate hazards of compound events

$$RP = \frac{E}{1 - F_{Q_c^q} - F_{t_c^q} + C\left(F_{Q_c^q}, F_{t_c^q}\right)} \tag{2}$$

where $F_{Q_c^q}(F_{t_c^q})$ is the marginal cumulative distribution of the excesses over a given quantile-based threshold. In consistent with previous studies (Zhou et al., 2019; Zscheischler & Seneviratne, 2017), we set the same exceedance probability for both the flood and hot extremes: $F_{Q_c^q} = F_{t_c^q}$. E denotes the average interarrival time between compound events.

In a warmer future climate, CFH hazards may potentially change in the world. The potential changes are principally caused by changes in floods, hot extremes, and their dependences. As suggested by Bevacqua et al. (2019), we carry out three experiments to disentangle the relative contributions of three drivers to changes in CFH hazards: (a) fixing the marginal distributions of hot extremes and the dependence between floods and hot extremes in the historical period and exchanging the marginal distributions of floods in the future period; (b) as experiment (a), but exchanging the marginal distributions of hot extremes in the future period; and (c) fixing both marginal distributions of floods and hot extremes in the historical period and using the fitted copula for the future period (more details see Text S1.5 in Supporting Information S1).

3. Results

3.1. Probability of Occurrence of Simulated and Projected CFHs

We identify the fractional contribution of CFH events (the fraction of CFHs to total flood events) across global and five broad Köppen-Geiger climate regions (Beck et al., 2018; Slater et al., 2021) under historical and future (SSP1-26, SSP2-45, SSP5-85) climates, respectively (Figure 1). From the global perspective, the fractional contributions of CFHs range from 0 to 1, with averaged values of 0.26 (historical), 0.41 (SSP1-26), 0.48 (SSP2-45), and 0.52 (SSP5-85). In terms of the distribution characteristics, the historical global fractional contribution broadly resembles a normal distribution with long lower and upper tails (Figure 1a). In the context of climate change, we find the distributions of global fractional contributions predominantly shift to the right, resulting in sharp increases in the occurrence of CFHs (Figures 1b–1d).

From the five climate zones, we find the fractional contributions are often highest in the polar zone, ranging between 0.30 and 0.63 in the historical climate (25th and 75th percentiles) and between 0.41 and 0.71 in the future

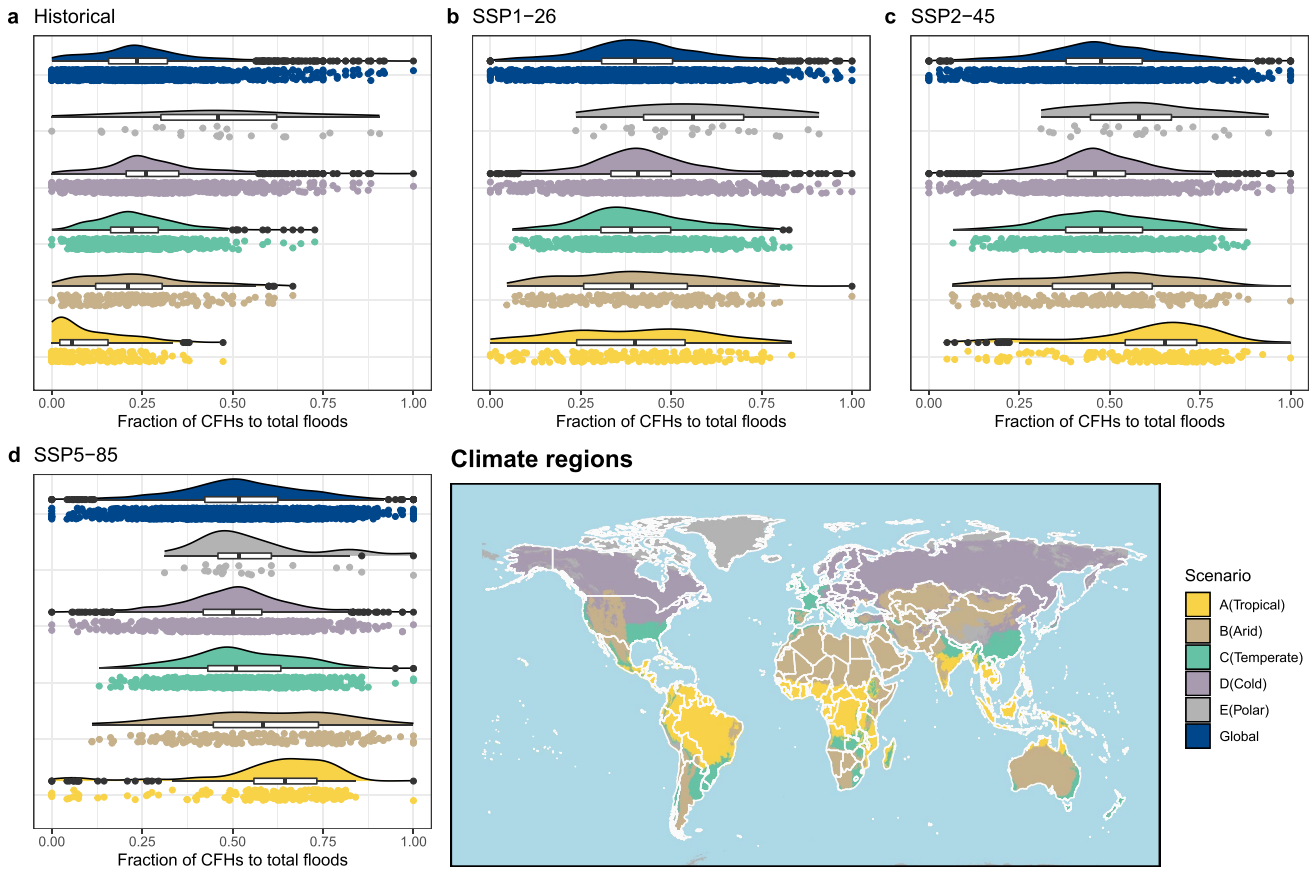

Figure 1. Raincloud plot showing the fraction of compound flood-hot extremes to total flood events across the five climate zones and the globe. (a) The fractions estimated during the historical 1985–2014 period. (b–d) The fractions projected during the future 2071–2100 period under the SSP1-26, SSP2-45, SSP5-85 scenarios, respectively. "Climate regions" display where each climate region is located on the globe. (To facilitate demonstration, catchments are not shown).

scenarios. In contrast, fractional contributions are smallest in the tropical region during the historical period, with an average fraction of only 0.12. However, they are projected to increase proportionally more than in any other climate zones in a warming future, with average fractions of 0.39 (SSP1-26) and 0.61 (SSP2-45 and SSP5-85). This suggests that a large portion of flooding will be accompanied by hot extremes across these tropical catchments, and the fractional contributions of CFHs will be greater compared to other climate zones. The historical fractional contributions in cold (0.24 on average), temperate (0.24), and arid (0.29) regions are moderate. These regions are expected to experience visible increases in fractional contributions, mostly becoming greater than 0.4.

Further, we examine the potential reasons behind these regional differences, especially the dramatic increases in fractional contributions across tropics and we find the main driver appears to be the change in frequency of hot extremes. The frequency change in hot extremes is projected to be more spatially heterogeneous than that in floods, resulting in these regional differences in fractional contribution change (Figure S12 in Supporting Information S1). For example, the frequency of hot extremes grows discernably faster than that of floods in tropics, favoring evident increases in fractional contributions over the tropics. In contrast, the frequency change in hot extremes is only slightly larger than in floods in polar regions, leading to weaker increases in local fractional contributions under global warming. In addition, we estimate the fraction of compound flood-hot extremes to total hot extremes (Figure S13 in Supporting Information S1). Projected increases in hot extremes fractions tend to be smaller than those in flood fractions because increases in the frequency are larger for hot extremes than for floods over majority catchments (Figure S14 in Supporting Information S1). Nevertheless, both fractions of CFHs to total floods and fractions of CFHs to total hot extremes are projected to increase and these increments are the most apparent in the tropical regions, followed by arid, temperate, and cold regions, and are the least apparent in the polar zone.

3.2. Projected Changes in CFH Hazards

Following the assessment of changes in the fractional contribution of CFH events, we focus on changes in their joint return periods. The evaluation of changes in joint return periods help understand the variations of joint magnitudes in floods and hot extremes, as well as their associated influences on the environment. In a warming future, we find joint return periods of compound extremes tend to decrease over 97% of catchments under three SSPs (Figure 2). These overall decreases in joint return periods occur irrespective of the level of warming, but are most prominent under the high emission scenario SSP5-85. In particular, historical (1985–2014) 30-year compound extremes are projected to become ~5-year events on average across all catchments over the 2071–2100 future period, under the SSP5-85 scenario. These changes to some degree mirror the changes in the fractional contribution of CFH events and indicate severely exacerbated CFH hazards under global warming.

Grouping these changes in joint return periods by climate zones provides further spatial information (Figures 2d–2f). Using the historical 30-year CFH event as a metric for detecting hazards, we find the most prominent decreases in joint return periods (increases in the frequency of CFH hazards) are projected to emerge in tropical catchments. Specifically, most tropical catchments are projected to see a sixfold increase in the frequency of CFH hazards, with moderate variations among the three emission scenarios (Figures 2d–2f). Catchments in other climate zones are also likely to face increasing frequency of CFH hazards, mostly varying from twofold to fivefold increases.

3.3. Drivers of Projected Changes in CFH Hazards

Changes in the joint return periods can, in principle, be attributed to changes in the marginal distributions of floods and hot extremes, as well as the interplay between both hazards. If only flood hazards were to change, we find the frequency of the projected CFH hazards would slightly increase (Figures 3a and 3d). For instance, on average at the global scale, the historical 30-year return period is projected to decrease to ~24 years under SSP2-45 (~24 years under SSP1-26 and ~23 years under SSP5-85; Figures S15 and S16 in Supporting Information S1). In contrast, the frequency of the projected CFH hazards drastically increase if only hot extremes were to change (Figures 3b and 3e). The historical 30-year return period is projected to decrease to ~12 years under the SSP2-45 scenario (~14 years under SSP1-26 and ~11 years under SSP5-85; Figures S15 and S16 in Supporting Information S1). Most global catchments are projected to experience strengthening dependence between floods and hot extremes (Figures S17 and S18 in Supporting Information S1), leading to weak and nonsignificant increases in the frequency of CFH hazards for majority catchments under all SSP scenarios (Figures 3c and 3f; Figures S15 and S16 in Supporting Information S1). Overall, contributions from hot extremes are the most significant and dominate changes in the frequency of CFH hazards, followed by contributions from floods with medium confidence, and finally the dependence showing the lowest confidence.

Regarding tropical catchments that show the highest increases in the frequency of CFH hazards, they are mainly controlled by changes in hot extremes. Changes in floods also contribute to the increasing frequency of CFH hazards, however, this contribution source seems not pronounced compared to other climate zones. Contributions from the strengthening dependence between floods and hot extremes are even smaller than those from floods for tropical catchments regardless that they are the highest among five climate zones. In addition, we also find that regional differences from hot extremes attribution are small. Specifically, hot extremes-induced changes in joint return periods over tropical catchments are no longer the largest among five climate zones as the global warming, indicating that the changes in the frequency of hot extremes hazards are not that relevant to spatial heterogeneity of changes in the frequency of CFH hazards. This is different from that in the fractional contributions in which frequency changes in hot extremes determine regional differences.

4. Discussion and Conclusion

Our findings indicate that the fraction of floods temporally compounded by hot extremes is projected to increase consistently across the majority of catchments in the context of climate change. This is consistent with previous studies that find CFH events are becoming more frequent under climate warming (Liao et al., 2021; Zhang & Villarini, 2020). Furthermore, we find that the bivariate CFH hazards could rise markedly under global warming, primarily due to enhancing hot extremes. The dominant role of changing hot extremes in exacerbating CFH hazards has been previously touched by Chen et al. (2021), though they only focus on China. Finally, we identify

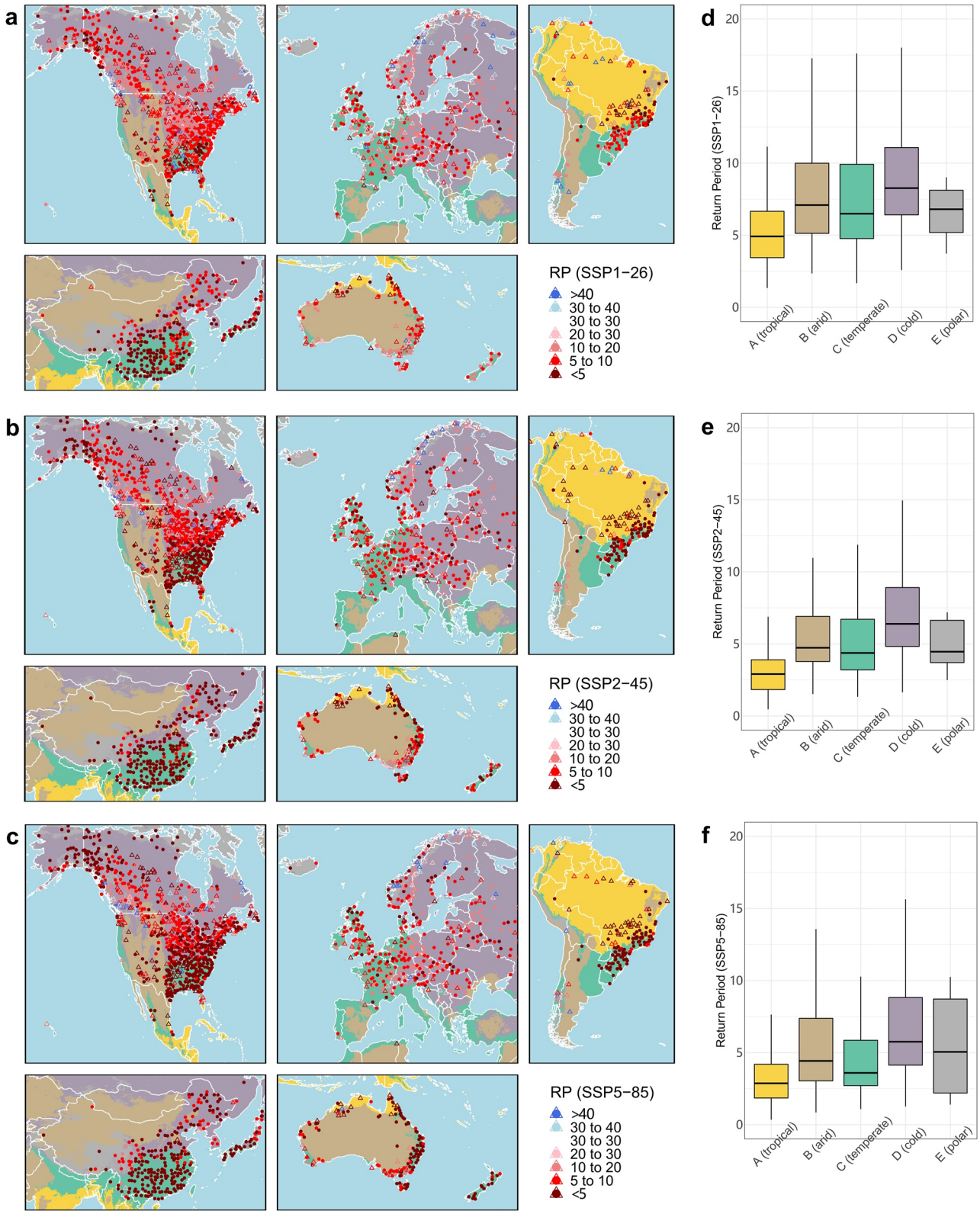

Figure 2.

the tropics as the new global hotspot of CFH hazards, attributed to synthesized impacts of changing hot extremes, floods, and dependences between both extremes. As these results suffer from multiple uncertainty sources, we first present the overall uncertainty in the indicators of compound events (i.e., the fraction of floods accompanied by hot extremes and the CFH hazards) in Figures S19 and S20 in Supporting Information S1. Generally, the uncertainty of the fraction of CFHs to total floods are minor relative to their multimodel ensemble mean (MMM) results (Figure S19 in Supporting Information S1), whereas the uncertainty of projected changes in the frequency of the CFH hazards are greater (Figure S20 in Supporting Information S1). We further examine relative contributions of uncertainty sources based on the ANOVA method (Bosshard et al., 2013). Only uncertainty from GCMs, emission scenarios and their interactions are considered in this study because uncertainty from other sources (e.g., bias correction method, hydrological models) are small according to previous work (Chen et al., 2013; Wang et al., 2020). Generally, GCMs cannot always explain most of uncertainty in these indicators (Figures S21 and S22 in Supporting Information S1), emission scenarios and their interactions are also important uncertainty sources. This highlights the necessity to use multiple GCMs and emission scenarios in evaluating climate change impacts on CFHs.

Further, to investigate whether multivariate bias correction can improve the ability of reproducing CFH relative to the univariate DBC method, we use five CMIP6 model outputs from the ISIMIP 3b based on a state-of-the-art multivariate bias adjustment technique (Lange, 2019) for comparison, and display their correlation relative to observations in Figure S23 in Supporting Information S1. The ISIMIP 3b results capture the dependence slightly better than the DBC method, but their improvements are quite limited. Moreover, we also investigate biases of the CFH characteristics in ISIMIP 3b and we find they cannot be effectively reduced relative to DBC (Figure S24 in Supporting Information S1). We infer the effectiveness of univariate bias adjustment might partly result from the good performance of the state-of-the-art CMIP6 outputs (Ridder et al., 2021). Nevertheless, it is possible that the robustness of DBC may not hold for other compound events or multivariate hazards (Zscheischler et al., 2019) and the effect of different bias correction techniques on compound hazard projections merits further investigation.

Some limitations must be highlighted. Deadly hot extremes can be identified by atmospheric dry bulb temperature, but they can also be based on wet bulb temperature which combines temperature and humidity (Im et al., 2017; Raymond et al., 2020). The next step of such an analysis will be to include the humidity factor affecting compound flood-hot extreme events, which is beyond the scope of this work. Different from existing studies, we take both sequences (flood-hot extreme and hot extreme-flood) into consideration from the impact perspective. However, it should be noted that different sequences involve different physical drivers and may response divergently to global warming. The flood-hot extreme sequence is typically linked with TCs and is prevalent in coastal regions, including southeast China, Japan, and northwest Australia (Liao et al., 2021; Matthews et al., 2019). With climate warming, the increasing frequency and intensity of TCs can be dominant drivers in altering this sequence of CFH hazards for these regions. Conversely, the hot extreme-flood sequence is usually related to the disturbed energy budget (e.g., increased sensible heat flux and convective available potential energy) after the onset of a hot extreme and has been studied in the central United States (Zhang & Villarini, 2020). Since global warming can lead to nonlinear increases in hot extremes, especially for tropical regions (Fischer & Knutti, 2015), increasing frequency of CFH hazards for these regions are predictable. Future studies can probe into the respective contributions of each sequence under the present climate and how they respond to anthropogenic warming separately.

Our study focuses on the spatiotemporal dynamics of meteorological and hydrological drivers of CFH events. Further, the projections of changing CFH events assessed herein are based on future changes in climate, but do not include other local factors such as land cover and land use changes, construction and operation of hydraulic infrastructure, and implementation of climate mitigation and adaptation strategies, which are commonly neglected in large-scale climate studies like the present. Therefore, our findings should be interpreted as a global assessment of changing frequency of CFH hazards in view of climate change, suggesting the need to increase community and societal resilience, particularly in tropical hotspots.

Figure 2. How might the historical 30-year joint CFH return period change by 2071–2100 under climate change? (a–c) Updated historical 30-year joint return period (RP) under the SSP1-26, SSP2-45, and SSP5-85 scenarios of compound flood-hot extreme (CFH). Red (blue) circles denote catchments with decreases (increases) in return periods. (d–f) Indicate the distributions of sites shown in (a)–(c), but grouped by five climate zones. A-E climate zones each contain 198, 212, 699, 996, 24 available catchments for each SSP, respectively. The filled circles (hollow triangles) indicate significant (nonsignificant) changes among 21 climate model ensembles using the sign-test at the $p = 0.05$ significance level.

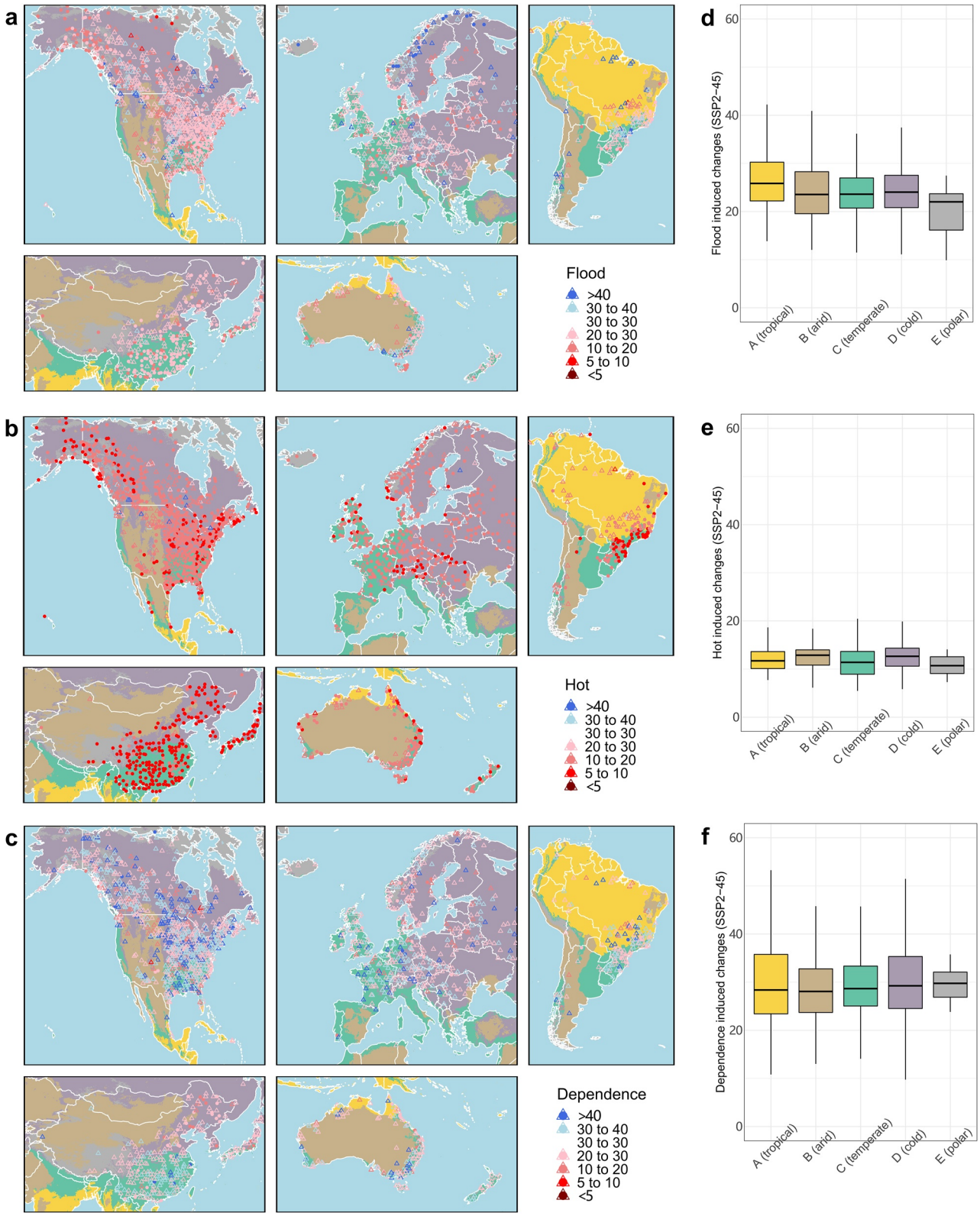

Figure 3. Flood-induced ("Flood"), hot extremes-induced ("Hot"), and dependence-induced ("Dependence") 30-year joint return period changes during 2071–2100 under the SSP2-45 scenario. Red (blue) circles denote decreases (increases) in return periods. The filled circles (hollow triangles) indicate significant (nonsignificant) changes among 21 climate model ensembles using the sign-test at the $p = 0.05$ significance level.

Conflict of Interest

The authors declare no conflicts of interest relevant to this study.

Data Availability Statement

The climate data in this study are available from (a) the ERA5 data can be downloaded from the website of ECMWF (https://www.ecmwf.int/en/forecasts/dataset/ecmwf-reanalysis-v5); (b) the CMIP6 outputs (see Table S1 in Supporting Information S1; https://esgf-node.llnl.gov/search/cmip6/); (c) the ISIMIP b3 data (see Table S2 in Supporting Information S1; https://data.isimip.org/search/tree/ISIMIP3b%2FInputData/); (d) the MSWEP V2 data (http://www.gloh2o.org/mswep/). The daily streamflow data and watershed boundaries (except Chinese watersheds) are publicly available and from (e) the Global River Discharge Centre (GRDC; https://www.bafg.de/GRDC/EN/Home/homepage_node.html; https://www.bafg.de/GRDC/EN/02_srvcs/22_gslrs/222_WSB/watershedBoundaries.html?nn=201570#Start); (f) the U.S. Geological Survey (USGS) National Water Information System (https://waterdata.usgs.gov/nwis/inventory?site_no=06904010; https://www.usgs.gov/national-hydrography/watershed-boundary-dataset); (g) the Australian Bureau of Meteorology (http://www.bom.gov.au/metadata/catalogue/19115/ANZCW0503900339?template=full; http://www.bom.gov.au/water/geofabric/about.shtml); (h) the UK Centre for Ecology and Hydrology (UKCEH; https://eip.ceh.ac.uk/hydrology/water-resources/; https://catalogue.ceh.ac.uk/documents/10d419c8-8f65-4b85-a78a-3d6e0485fa1f); (i) the Environment and Climate Change Canada (ECCC) through the Water Survey of Canada (WSC; https://wateroffice.ec.gc.ca/search/historical_e.html; https://open.canada.ca/data/en/dataset/a4b190fe-e090-4e6d-881e-b87956c07977); (j) the Brazilian National Water Agency (ANA; http://www.snirh.gov.br/hidroweb/apresentacao; Since Brazil does not provide official database of national catchments boundaries, the Brazilian catchment boundaries were generated by using the digital elevation model (DEM) and ARC-INFO GRID module); (k) the Ministry of Water Resources of China (both streamflow data and watershed boundaries need Chinese credentials and are not publicly available). Simulated streamflow data in this study are available at the repository in the Open Science Framework (https://osf.io/j4mwu/?view_only=ade751a6aa3147f78e992cbb96e792c5).

Acknowledgments

This work was supported by the National Key Research and Development Program of China (2021YFC3200301), the Guangdong Provincial Department of Science and Technology (2019ZT08G090), the National Natural Science Foundation of China (51779176), the National Natural Science Foundation of China (52009091), UK Research and Innovation (MR/V022008/1 to L.S.), the Fundamental Research Funds for the Central Universities (2021XXJS077), and the Natural Science Foundation of Hubei Province (2020CFB239). The authors would like to thank the World Climate Research Program working group on Coupled Modelling and all climate modeling institutions for making climate model outputs available. Also, we acknowledge the ECMWF for providing the ERA5 reanalysis data set and the GloH2O for making the MSWEP V2 data available, and GRDC, USGS, UKCEH, ECCC, WSC, ANA and the Ministry of Water Resources of China for providing the streamflow gauge records.

References

Akaike, H. (1974). A new look at the statistical model identification. *IEEE Transactions on Automatic Control*, *19*(6), 716–723.

Almagro, A., Oliveira, P. T. S., & Brocca, L. (2021). Assessment of bottom-up satellite rainfall products on estimating river discharge and hydrologic signatures in Brazilian catchments. *Journal of Hydrology*, *160*, 126897.

Arsenault, R., Essou, G. R., & Brissette, F. P. (2017). Improving hydrological model simulations with combined multi-input and multi-model averaging frameworks. *Journal of Hydrologic Engineering*, *22*(4), 04016066.

Bardon, L. R., Ward, B. A., Dutkiewicz, S., & Cael, B. B. (2021). Testing the skill of a species distribution model using a 21st century virtual ecosystem. *Geophysical Research Letters*, *48*, e2021GL093455. https://doi.org/10.1029/2021GL093455

Beck, H. E., Wood, E. F., Pan, M., Fisher, C. K., Miralles, D. G., Van Dijk, A. I., et al. (2019). MSWEP V2 global 3-hourly 0.1 precipitation: Methodology and quantitative assessment. *Bulletin of the American Meteorological Society*, *100*(3), 473–500.

Beck, H. E., Zimmermann, N. E., McVicar, T. R., Vergopolan, N., Berg, A., & Wood, E. F. (2018). Present and future Köppen-Geiger climate classification maps at 1-km resolution. *Scientific Data*, *5*, 180214. https://doi.org/10.1038/sdata.2018.214

Berg, A., Lintner, B. R., Findell, K., Seneviratne, S. I., van den Hurk, B., Ducharne, A., et al. (2015). Interannual coupling between summertime surface temperature and precipitation over land: Processes and implications for climate change. *Journal of Climate*, *28*, 1308–1328.

Bergström, S., & Forsman, A. (1973). Development of a conceptual deterministic rainfall-runoff mode. Nord. *Hydrology*, *4*, 240–253.

Bevacqua, E., Maraun, D., Vousdoukas, M. I., Voukouvalas, E., Vrac, M., Mentaschi, L., & Widmann, M. (2019). Higher probability of compound flooding from precipitation and storm surge in Europe under anthropogenic climate change. *Science Advances*, *5*(9), eaaw5531. https://doi.org/10.1126/sciadv.aaw5531

Bosshard, T., Carambia, M., Goergen, K., Kotlarski, S., Krahe, P., Zappa, M., & Schär, C. (2013). Quantifying uncertainty sources in an ensemble of hydrological climate-impact projections. *Water Resources Research*, *49*, 1523–1536. https://doi.org/10.1029/2011WR011533

Brida, A. B., Owiyo, T., & Sokona, Y. (2013). Loss and damage from the double blow of flood and drought in Mozambique. *International Journal of Global Warming*, *5*(4), 514–531.

Cai, W., McPhaden, M. J., Grimm, A. M., Rodrigues, R. R., Taschetto, A. S., Garreaud, R. D., et al. (2020). Climate impacts of the El Niño-Southern oscillation on South America. *Nature Reviews Earth & Environment*, *1*, 215–231.

Cappucci, M. (2019). *Storms deluge New York City, abruptly ending sweltering heat wave*. Retrieved from https://www.washingtonpost.com/weather/2019/07/23/flooding-rain-deluges-new-york-city-abruptly-ending-sweltering-heat-wave/

Chen, H., Wang, S., & Wang, Y. (2020). Exploring abrupt alternations between wet and dry conditions on the basis of historical observations and convection-permitting climate model simulations. *Journal of Geophysical Research: Atmospheres*, *125*, e2019JD031982. https://doi.org/10.1029/2019JD031982

Chen, J., Brissette, F. P., Chaumont, D., & Braun, M. (2013). Finding appropriate bias correction methods in downscaling precipitation for hydrologic impact studies over North America. *Water Resources Research*, *49*, 4187–4205. https://doi.org/10.1002/wrcr.20331

Chen, Y., Liao, Z., Shi, Y., Tian, Y., & Zhai, P. (2021). Detectable increases in sequential flood-heatwave events across China during 1961–2018. *Geophysical Research Letters*, *48*, e2021GL092549. https://doi.org/10.1029/2021GL092549

Chen, Y., & Zhai, P. (2017). Simultaneous modulations of precipitation and temperature extremes in Southern parts of China by the boreal summer intraseasonal oscillation. *Climate Dynamics*, *49*(9–10), 3363–3381.
Chiew, F. H. S., Peel, M. C., & Western, A. W. (2002). Application and testing of the simple rainfall-runoff model SIMHYD. In *Mathematical models of small watershed hydrology and applications* (pp. 335–367).
Courty, L. G., Wilby, R. L., Hillier, J. K., & Slater, L. J. (2019). Intensity-duration-frequency curves at the global scale. *Environmental Research Letters*, *14*(8), 084045.
Cowan, T., Wheeler, M. C., Alves, O., Narsey, S., de Burgh-Day, C., Griffiths, M., et al. (2019). Forecasting the extreme rainfall, low temperatures, and strong winds associated with the northern Queensland floods of February 2019. *Weather and Climate Extremes*, *26*, 100232.
Deng, K., Jiang, X., Hu, C., & Chen, D. (2020). More frequent summer heat waves in southwestern China linked to the recent declining of Arctic Sea ice. *Environmental Research Letters*, *15*(7), 074011.
Do, H. X., Westra, S., Leonard, M., & Gudmundsson, L. (2020). Global-scale prediction of flood timing using atmospheric reanalysis. *Water Resources Research*, *56*, e2019WR024945. https://doi.org/10.1029/2019WR024945
Duan, Q., Sorooshian, S., & Gupta, V. (1992). Effective and efficient global optimization for conceptual rainfall-runoff models. *Water Resources Research*, *28*(4), 1015–1031.
Enomoto, T., Endo, H., Harada, Y., & Ohfuchi, W. (2009). Relationship between high-impact weather events in Japan and propagation of Rossby waves along the Asian jet in July 2004. *Journal of the Meteorological Society of Japan. Ser. II*, *87*(1), 139–156.
Fischer, E. M., & Knutti, R. (2015). Anthropogenic contribution to global occurrence of heavy-precipitation and high-temperature extremes. *Nature Climate Change*, *5*(6), 560–564.
Fowler, H. J., Lenderink, G., Prein, A. F., Westra, S., Allan, R. P., Ban, N., et al. (2021). Anthropogenic intensification of short-duration rainfall extremes. *Nature Reviews Earth & Environment*, *2*, 1–122.
Gu, L., Chen, J., Yin, J., Xu, C. Y., & Zhou, J. (2020). Responses of precipitation and runoff to climate warming and implications for future drought changes in China. *Earth's Future*, *8*, e2020EF001718. https://doi.org/10.1029/2020EF001718
Gu, L., Yin, J., Zhang, H., Wang, H. M., Yang, G., & Wu, X. (2021). On future flood magnitudes and estimation uncertainty across 151 catchments in mainland China. *International Journal of Climatology*, *41*, E779–E800.
Gupta, H. V., Kling, H., Yilmaz, K. K., & Martinez, G. F. (2009). Decomposition of the mean squared error and NSE performance criteria: Implications for improving hydrological modelling. *Journal of Hydrology*, *377*(1–2), 80–91.
Hersbach, H., Bell, B., Berrisford, P., Hirahara, S., Horányi, A., Muñoz-Sabater, J., et al. (2020). The ERA5 global reanalysis. *Quarterly Journal of the Royal Meteorological Society*, *146*(730), 1999–2049.
Im, E. S., Pal, J. S., & Eltahir, E. A. B. (2017). Deadly heat waves projected in the densely populated agricultural regions of South Asia. *Science Advances*, *3*(8), e1603322. https://doi.org/10.1126/sciadv.1603322
Jiang, L., Wu, H., Tao, J., Kimball, J. S., Alfieri, L., & Chen, X. (2020). Satellite-based evapotranspiration in hydrological model calibration. *Remote Sensing*, *12*(3), 428.
Kemter, M., Merz, B., Marwan, N., Vorogushyn, S., & Blöschl, G. (2020). Joint trends in flood magnitudes and spatial extents across Europe. *Geophysical Research Letters*, *47*, e2020GL087464. https://doi.org/10.1029/2020GL087464
Lange, S. (2019). Trend-preserving bias adjustment and statistical downscaling with ISIMIP3BASD (v1.0). *Geoscientific Model Development*, *12*, 3055–3070. https://doi.org/10.5194/gmd-12-3055-2019
Liao, Z., Chen, Y., Li, W., & Zhai, P. (2021). Growing threats from unprecedented sequential flood-hot extremes across China. *Geophysical Research Letters*, *48*, e2021GL094505. https://doi.org/10.1029/2021GL094505
Lin, N. (2019). Tropical cyclones and heatwaves. *Nature Climate Change*, *9*(8), 579–580.
Martel, J. L., Demeester, K., Brissette, F. P., Arsenault, R., & Poulin, A. (2017). HMET: A simple and efficient hydrology model for teaching hydrological modelling, flow forecasting and climate change impacts. *International Journal of Engineering Education*, *33*(4), 1307–1316.
Matthews, T., Wilby, R. L., & Murphy, C. (2019). An emerging tropical cyclone-deadly heat compound hazard. *Nature Climate Change*, *9*(8), 602–606.
Menne, M. J., Williams, C. N., Gleason, B. E., Rennie, J. J., & Lawrimore, J. H. (2018). The global historical climatology network monthly temperature dataset, version 4. *Journal of Climate*, *31*(24), 9835–9854.
Mukherjee, S., & Mishra, A. K. (2021). Increase in compound drought and heatwaves in a warming world. *Geophysical Research Letters*, *48*, e2020GL090617. https://doi.org/10.1029/2020GL090617
Parker, T. J., Berry, G. J., & Reeder, M. J. (2013). The influence of tropical cyclones on heat waves in Southeastern Australia. *Geophysical Research Letters*, *40*, 6264–6270. https://doi.org/10.1002/2013GL058257
Pendergrass, A. G., & Knutti, R. (2018). The uneven nature of daily precipitation and its change. *Geophysical Research Letters*, *45*, 11980–11988. https://doi.org/10.1029/2018GL080298
Perrin, C., Michel, C., & Andreassian, V. (2003). Improvement of a parsimonious model for streamflow simulation. *Journal of Hydrology*, *279*, 275–289.
Raghavendra, A., Dai, A., Milrad, S. M., & Cloutier-Bisbee, S. R. (2019). Floridian heatwaves and extreme precipitation: Future climate projections. *Climate Dynamics*, *52*(1), 495–508.
Raymond, C., Matthews, T., & Horton, R. M. (2020). The emergence of heat and humidity too severe for human tolerance. *Science Advances*, *6*(19), eaaw1838. https://doi.org/10.1126/sciadv.aaw1838
Rhoades, A. M., Jones, A. D., Srivastava, A., Huang, H., O'Brien, T. A., Patricola, C. M., et al. (2020). The shifting scales of Western US landfalling atmospheric rivers under climate change. *Geophysical Research Letters*, *47*, e2020GL089096. https://doi.org/10.1029/2020GL089096
Ridder, N. N., Pitman, A. J., & Ukkola, A. M. (2021). Do CMIP6 climate models simulate global or regional compound events skillfully?*Geophysical Research Letters*, *48*, e2020GL091152. https://doi.org/10.1029/2020GL091152
Ridder, N. N., Pitman, A. J., Westra, S., Ukkola, A., Do, H. X., Bador, M., et al. (2020). Global hotspots for the occurrence of compound events. *Nature Communications*, *11*(1), 5956.
Schumacher, D. L., Keune, J., van Heerwaarden, C. C., Vilà-Guerau de Arellano, J., Teuling, A. J., & Miralles, D. G. (2019). Amplification of mega-heatwaves through heat torrents fuelled by upwind drought. *Nature Geoscience*, *12*, 712–717.
Shi, H., García-Reyes, M., Jacox, M. G., Rykaczewski, R. R., Black, B. A., Bograd, S. J., & Sydeman, W. J.. (2021). Co-occurrence of California drought and Northeast Pacific marine heatwaves under climate change. *Geophysical Research Letters*, *48*, e2021GL092765. https://doi.org/10.1029/2021GL092765
Slater, L., Villarini, G., Archfield, S., Faulkner, D., Lamb, R., Khouakhi, A., & Yin, J. (2021). Global changes in 20-year, 50-year, and 100-year river floods. *Geophysical Research Letters*, *48*, e2020GL091824. https://doi.org/10.1029/2020GL091824
Thiessen, A. H., & Alter, J. C. (1911). Precipitation averages for large areas. *Monthly Weather Review*, *39*(7), 1082–1089.

Wang, H. M., Chen, J., Xu, C. Y., Zhang, J., & Chen, H. (2020). A framework to quantify the uncertainty contribution of GCMs over multiple sources in hydrological impacts of climate change. *Earth's Future*, *8*, e2020EF001602. https://doi.org/10.1029/2020EF001602

Wang, S. S. Y., Kim, H., Coumou, D., Yoon, J. H., Zhao, L., & Gillies, R. R. (2019). Consecutive extreme flooding and heat wave in Japan: Are they becoming a norm?*Atmospheric Science Letters*, *20*(10), e933. https://doi.org/10.1002/asl.933

Yin, J., Guo, S., Gentine, P., Sullivan, S. C., Gu, L., He, S., et al. (2021). Does the hook structure constrain future flood intensification under anthropogenic climate warming. *Water Resources Research*, *57*, e2020WR028491. https://doi.org/10.1029/2020WR028491

Yin, J., Guo, S., Gu, L., Zeng, Z., Liu, D., Chen, J., et al. (2021). Blending multi-satellite, atmospheric reanalysis and gauge precipitation products to facilitate hydrological modelling. *Journal of Hydrology*, *593*, 125878.

You, J., & Wang, S. (2021). Higher probability of occurrence of hotter and shorter heat waves followed by heavy rainfall. *Geophysical Research Letters*, *48*, e2021GL094831. https://doi.org/10.1029/2021GL094831

Zhang, W., & Villarini, G. (2020). Deadly compound heat stress-flooding hazard across the central United States. *Geophysical Research Letters*, *47*, e2020GL089185. https://doi.org/10.1029/2020GL089185

Zhao, R. J. (1992). The Xinanjiang model applied in China. *Journal of Hydrology*, *135*(1), 371–381.

Zhou, S., Williams, A. P., Berg, A. M., Cook, B. I., Zhang, Y., Hagemann, S., et al. (2019). Land–atmosphere feedbacks exacerbate concurrent soil drought and atmospheric aridity. *Proceedings of the National Academy of Sciences of the United States of America*, *116*(38), 18848–18853.

Zscheischler, J., & Fischer, E. M. (2020). The record-breaking compound hot and dry 2018 growing season in Germany. *Weather and Climate Extremes*, *29*, 100270.

Zscheischler, J., Fischer, E. M., & Lange, S. (2019). The effect of univariate bias adjustment on multivariate hazard estimates. *Earth System Dynamics*, *10*(1), 31–43.

Zscheischler, J., & Lehner, F. (2021). Attributing compound events to anthropogenic climate change. *Bulletin of the American Meteorological Society*, *1*(aop), 1–45.

Zscheischler, J., Martius, O., Westra, S., Bevacqua, E., Raymond, C., Horton, R. M., et al. (2020). A typology of compound weather and climate events. *Nature Reviews Earth & Environment*, *1*(7), 333–347.

Zscheischler, J., & Seneviratne, S. I. (2017). Dependence of drivers affects risks associated with compound events. *Science Advances*, *3*(6), e1700263.

References From the Supporting Information

Nelsen, R. B. (2007). *An introduction to copulas*. Springer Science & Business Media.

Su, T., Chen, J., Cannon, A. J., Xie, P., & Guo, Q. (2020). Multi-site bias correction of climate model outputs for hydro-meteorological impact studies: An application over a watershed in China. *Hydrological Processes*, *34*(11), 2575–2598.